Massive MIMO Joint Communications and Sensing with MRT Beamforming

Nhan T. Nguyen*, V.-Dinh Nguyen†, Hieu V. Nguyen‡, Hien Q. Ngo§, A. L. Swindlehurst¶, Markku Juntti*
*Centre for Wireless Communications, University of Oulu, P.O.Box 4500, FI-90014, Finland
†College of Engineering and Computer Science, VinUniversity, Hanoi, Vietnam
‡Faculty of Electronics and Telecommunication Engineering, University of Danang, Vietnam
§School of Electronics, Electrical Engineering and Computer Science, Queen's University Belfast, UK
¶Center for Pervasive Communications & Computing, University of California, Irvine, CA, USA
Email: {nhan.nguyen, markku.juntti}@oulu.fi; dinh.nv2@vinuni.edu.vn, nvhieu@dut.udn.vn, hien.ngo@qub.ac.uk, swindle@uci.edu

2024 IEEE Radar Conference (RadarConf24) | 979-8-3503-2920-9/24/$31.00 ©2024 IEEE | DOI: 10.1109/RADARCONF2458775.2024.10549340

***Abstract*—Joint communications and sensing (JCAS) is envisioned as a key feature in future wireless communications networks. In massive MIMO-JCAS systems, the very large number of antennas causes excessively high computational complexity in beamforming designs. In this work, we investigate a low-complexity massive multiple-input-multiple-output (MIMO)-JCAS system employing the maximum-ratio transmission (MRT) scheme for both communications and sensing. We first derive closed-form expressions for the achievable communications rate and Cramér–Rao bound (CRB) as functions of the large-scale fading channel coefficients. Then, we develop a power allocation strategy based on successive convex approximation to maximize the communications sum rate while guaranteeing the CRB constraint and transmit power budget. Our analysis shows that the introduction of sensing functionality increases the beamforming uncertainty and inter-user interference on the communications side. However, these factors can be mitigated by deploying a very large number of antennas. The numerical results verify our findings and demonstrate the power allocation efficiency.**

***Index Terms*—Joint communications and sensing (JCAS), massive MIMO, maximum-ratio transmission.**

I. Introduction

Joint communications and sensing (JCAS) has emerged as a potential technology for future wireless communication systems [1]. Thus, transmit beamforming design for JCAS systems is the focus of growing attention in recent literature [2]–[5]. In [2]–[4], the transmit beamformers were designed to minimize the beampattern error constrained by the communications signal-to-interference-plus-noise ratio (SINR). A reliable transmit beampattern guarantees that the sensed targets and communications users are covered at the same time, while minimizing the Cramér–Rao bound (CRB) ensures consideration of the estimation quality of the sensed parameters [3], [6], [7]. Other SINR-based merit functions for sensing are introduced and investigated in [4]. In most of these existing works, small-sized antenna arrays were employed for the JCAS transmission. This does not ensure high spatial beamforming gains, and hence limits both sensing and communications performance.

Compared to conventional multiple-input-multiple-output (MIMO) communications, massive MIMO technology employing very large arrays offers superior spectral and energy efficiency (SE/EE) for communications systems [8]–[10]. Recent literature has shown that massive MIMO is also promising for JCAS systems. Specifically, it has been shown in [11] that by leveraging a massive MIMO radar-base station (BS), the communications and radar systems can coexist with little mutual interference. Temiz *et al.* [12] proposed a joint uplink massive MIMO communications and orthogonal frequency-division multiplexing (OFDM) radar sensing architecture, wherein zero-forcing (ZF) and ordered successive interference cancellation (OSIC) receivers are used to eliminate the inter-user and radar interference during communications symbol detection. In [13]–[16], the radar performance of massive MIMO systems is optimized under constraints on communications performance. On the other hand, the communications rate of massive MIMO-JCAS systems is maximized in [17]–[19] subject to constraints on the radar performance. While these works all consider large or massive MIMO configurations, the system design and optimization are complicated and are conducted only over small-scale intervals. However, owing to its large number of degrees of freedom, massive MIMO can provide good communications performance with simple linear beamforming methods such as maximum-ratio transmission (MRT) and ZF [20].

In this work, we consider a mono-static multiuser massive MIMO-JCAS system employing the MRT precoder. We first derive closed-form expressions for the achievable sum rate and the CRB as the performance metrics for the downlink communications and the sensed target estimation, respectively. These allow us to characterize the important properties of the communications and sensing operations in massive MIMO scenarios. Specifically, they show that the sensing objective increases the MRT beamforming uncertainty and the inter-user interference of the communications channels. However, these drawbacks can be mitigated by deploying a very large number of antennas. Then, we focus on the use of power allocation to maximize the communications sum rate while constraining the CRB. The formulated problem is nonconvex, but we develop an efficient solution leveraging the successive convex approximation (SCA) approach. Finally, we provide numerical results to verify our theoretical findings and demonstrate the performance of the power allocation scheme.

II. Signal Model

We consider a mono-static massive MIMO JCAS system, including a base station (BS), K single-antenna communications users, and a sensed target. We assume that the BS is equipped

with $N_{\mathtt{t}}$ transmit and $N_{\mathtt{r}}$ receive antennas, with $N_{\mathtt{t}}+N_{\mathtt{r}} \gg 1$. At the BS, the $N_{\mathtt{t}}$ antennas simultaneously transmit probing signals to the target at a given angle of interest and data signals to the users. The echo from the sensed target is then processed by the $N_{\mathtt{r}}$ receive antennas at the BS.

A. Communications Model

1) Signal Model: Denote by $\mathbf{s}_\ell = [s_{1\ell}, \ldots, s_{k\ell}, \ldots, s_{K\ell}] \in \mathbb{C}^{K\times 1}$ the transmit vector from the BS at the ℓ-th time slot, with $\mathbb{E}\{\mathbf{s}_\ell \mathbf{s}_\ell^{\mathsf{H}}\} = \mathbf{I}_K$. Here we assume that $s_{k\ell}$ is the signal intended for the k-th user. Furthermore, let $\mathbf{S} = [\mathbf{s}_1, \ldots, \mathbf{s}_L] \in \mathbb{C}^{K\times L}$ be the transmit symbol matrix, where $L \gg 1$ is the length of the radar/communications frame. The data streams are assumed to be independent of each other such that

$$\mathbf{S}\mathbf{S}^{\mathsf{H}} \approx L\mathbf{I}_K, \tag{1}$$

which holds asymptotically for Gaussian signaling when L is sufficiently large [6].

The BS employs the linear precoder

$$\mathbf{F} = \mathbf{W}\mathbf{\Gamma} + \mathbf{v}\bar{\boldsymbol{\eta}}^{\mathsf{T}} \in \mathbb{C}^{N_{\mathtt{t}}\times K}, \tag{2}$$

where $\mathbf{W} = [\mathbf{w}_1, \ldots, \mathbf{w}_K] \in \mathbb{C}^{N_{\mathtt{t}}\times K}$ and $\mathbf{\Gamma} = \mathtt{diag}\left\{\sqrt{\gamma_1}, \ldots, \sqrt{\gamma_K}\right\} \in \mathbb{C}^{K\times K}$ are the matrix of precoding vectors and power allocation factors for communications users. Specifically, $\mathbf{w}_k$ and γ_k are the precoding vector and power allocated for the kth communications user, with $\|\mathbf{w}_k\|^2 = 1, \forall k$. On the other hand, $\mathbf{v} \in \mathbb{C}^{N_{\mathtt{t}}\times 1}$ and $\bar{\boldsymbol{\eta}} = [\sqrt{\eta_1}, \ldots, \sqrt{\eta_K}]^{\mathsf{T}} \in \mathbb{C}^{K\times 1}$ are the precoding vector and power fraction allocated for sensing in each communication stream. The k-th column $\mathbf{F}$, denoted as $\mathbf{f}_k$, represents the dual-functional precoding vector for user k and is given as $\mathbf{f}_k = \sqrt{\gamma_k}\mathbf{w}_k + \sqrt{\eta_k}\mathbf{v}$. Then, the $N_{\mathtt{t}} \times 1$ transmit signal vector during the ℓ-th time slot is $\mathbf{x}_\ell = \mathbf{F}\mathbf{s}_\ell = \sum_{k=1}^{K} \mathbf{f}_k s_{k\ell}$, and the overall dual-functional transmit waveform is denoted by $\mathbf{X} = [\mathbf{x}_1, \ldots, \mathbf{x}_L] \in \mathbb{C}^{N_{\mathtt{t}}\times L}$. Equivalently, we have $\mathbf{X} = \mathbf{F}\mathbf{S}$.

For transmit waveform $\mathbf{X}$, the $K\times L$ combined signal matrix received by the users can be expressed as

$$\mathbf{Y} = \mathbf{H}^{\mathsf{H}}\mathbf{X} + \mathbf{N} = \mathbf{H}^{\mathsf{H}}\mathbf{F}\mathbf{S} + \mathbf{N}, \tag{3}$$

where $\mathbf{N} \in \mathbb{C}^{K\times L}$ is additive white Gaussian noise (AWGN) with independent entries following distribution $\mathcal{CN}(0, \sigma_{\mathtt{u}}^2)$, and $\mathbf{H} = [\mathbf{h}_1, \ldots, \mathbf{h}_k, \ldots, \mathbf{h}_K] \in \mathbb{C}^{N_{\mathtt{t}}\times K}$ is the channel matrix from the BS to the K users. Here, $\mathbf{h}_k$ denotes the channel between the BS and the k-th user and is given as [21]

$$\mathbf{h}_k = \beta_k^{1/2}\bar{\mathbf{h}}_k, \tag{4}$$

where β_k and $\bar{\mathbf{h}}_k$ represent the large-scale fading parameter and the small-scale Rayleigh fading channels, respectively.

The received signal at user k over L time slots is given as $\mathbf{y}_k^{\mathsf{T}} = \mathbf{h}_k^{\mathsf{H}}\mathbf{F}\mathbf{S} + \mathbf{n}_k^{\mathsf{T}} \in \mathbb{C}^{1\times L}$. Equivalently, at the ℓ-th time slot, the received signal at user k is

$$y_{k\ell} = \mathbf{h}_k^{\mathsf{H}}\mathbf{f}_k s_{k\ell} + \mathbf{h}_k^{\mathsf{H}} \sum\nolimits_{j\neq k} \mathbf{f}_j s_{\ell j} + n_{k\ell}. \tag{5}$$

2) Communications Channel Estimation: We assume a time-division duplex (TDD) protocol for the considered JCAS system. Specifically, the channel is first estimated via uplink training, which is then used for the downlink transmission. Let $\tau_{\mathtt{c}}$ be the length of the coherence interval in samples, and let $\tau_{\mathtt{p}} < \tau_{\mathtt{c}}$ be the length of the pilot sequences. The pilot sequence for the kth user is $\sqrt{\tau_{\mathtt{p}}}\boldsymbol{\psi}_k \in \mathbb{C}^{\tau_{\mathtt{p}}\times 1}$, and the MMSE channel estimate is given by

$$\hat{\mathbf{h}}_k = \frac{\sqrt{\tau_{\mathtt{p}} p_{\mathtt{p}}}\beta_k}{\tau_{\mathtt{p}} p_{\mathtt{p}} \sum_{j=1}^{K} \beta_j \left|\boldsymbol{\psi}_j^{\mathsf{H}}\boldsymbol{\psi}_k\right|^2 + \sigma_{\mathtt{u}}^2} \mathbf{Y}_{\mathtt{p}}\boldsymbol{\psi}_k, \tag{6}$$

where $\mathbf{Y}_{\mathtt{p}} = \sqrt{\tau_{\mathtt{p}} p_{\mathtt{p}}} \sum_{k=1}^{K} \mathbf{h}_k \boldsymbol{\psi}_k^{\mathsf{H}} + \mathbf{N}_{\mathtt{p}}$ is the received pilot signal at the BS during uplink training, and $p_{\mathtt{p}}$ is the average power of the training symbols. Furthermore, we have $\hat{\mathbf{h}}_k \sim \mathcal{CN}(0, \xi_k \mathbf{I}_{N_{\mathtt{t}}})$, with

$$\xi_k = \frac{\tau_{\mathtt{p}} p_{\mathtt{p}} \beta_k^2}{\tau_{\mathtt{p}} p_{\mathtt{p}} \sum_{j=1}^{K} \beta_j \left|\boldsymbol{\psi}_j^{\mathsf{H}}\boldsymbol{\psi}_k\right|^2 + \sigma_{\mathtt{u}}^2}. \tag{7}$$

The channel estimation error associated with $\hat{\mathbf{h}}_k$ is $\mathbf{e}_k = \mathbf{h}_k - \hat{\mathbf{h}}_k$, which is independent of $\hat{\mathbf{h}}_k$, and $\mathbf{e}_k \sim \mathcal{CN}(0, \epsilon_k \mathbf{I}_{N_{\mathtt{t}}})$ with

$$\epsilon_k \triangleq \beta_k - \xi_k = \frac{\beta_k \left(\tau_{\mathtt{p}} p_{\mathtt{p}} \sum_{j\neq k} \beta_j \left|\boldsymbol{\psi}_j^{\mathsf{H}}\boldsymbol{\psi}_k\right|^2 + \sigma_{\mathtt{u}}^2\right)}{\tau_{\mathtt{p}} p_{\mathtt{p}} \sum_{j=1}^{K} \beta_j \left|\boldsymbol{\psi}_j^{\mathsf{H}}\boldsymbol{\psi}_k\right|^2 + \sigma_{\mathtt{u}}^2}. \tag{8}$$

B. Radar Sensing Model

The BS receives and processes the echo signals from the target for sensing functions such as detection and estimation. The discrete-time radar signal received at the BS is given as

$$\tilde{\mathbf{Y}} = \alpha \mathbf{A}(\theta)\mathbf{X} + \tilde{\mathbf{N}}, \tag{9}$$

where $\tilde{\mathbf{N}} \in \mathbb{C}^{N_{\mathtt{r}}\times L}$ is an AWGN matrix with independent entries distributed as $\mathcal{CN}(0, \sigma_{\mathtt{r}}^2)$. In (9), $\mathbf{A}(\theta) \in \mathbb{C}^{N_{\mathtt{r}}\times N_{\mathtt{t}}}$ is the two-way channel in the desired sensing directions. We assume that the BS employs a uniform linear array (ULA) with half-wavelength antenna spacing. The channel $\mathbf{A}(\theta)$ in (9) can be modeled as $\mathbf{A}(\theta) = \mathbf{a}_{\mathtt{r}}(\theta)\mathbf{a}_{\mathtt{t}}^{\mathsf{H}}(\theta)$, where θ is the angle of the target relative to the BS, and $\mathbf{a}_{\mathtt{t}}(\theta)$ and $\mathbf{a}_{\mathtt{r}}(\theta)$ are the steering vectors associated with the transmit and receive arrays [3], [4]. To simplify the notation, we assume an even number of antennas and choose the center of the ULA as the reference point, such that and have [6]

$$\mathbf{a}_{\mathtt{x}}(\theta) = \left[e^{-j\frac{N_{\mathtt{x}}-1}{2}\pi\sin(\theta)}, e^{-j\frac{N_{\mathtt{x}}-3}{2}\pi\sin(\theta)}, \ldots, e^{j\frac{N_{\mathtt{x}}-1}{2}\pi\sin(\theta)}\right]^{\mathsf{T}}, \tag{10}$$

where $\mathtt{x} \in \{\mathtt{t}, \mathtt{r}\}$. In the following analysis, we drop (θ) for further simplicity.

III. Performance of Massive MIMO JCAS Systems with MRT Beamforming

In this section, we derive lower bounds on the achievable sum rate of the communications subsystem that employs linear MRT transmit beamforming. For the sensing subsystem, we derive the CRB to evaluate the estimation accuracy.

First, to formulate the MRT precoder, based on (2) we rewrite (9) as

$$\tilde{\mathbf{Y}} = \alpha \mathbf{a}_{\mathtt{r}}\mathbf{a}_{\mathtt{t}}^{\mathsf{H}} \left(\mathbf{W}\mathbf{\Gamma} + \mathbf{v}\bar{\boldsymbol{\eta}}^{\mathsf{T}}\right)\mathbf{S} + \tilde{\mathbf{N}} = \alpha \mathbf{a}_{\mathtt{r}}\mathbf{a}_{\mathtt{t}}^{\mathsf{H}}\mathbf{v}\bar{\boldsymbol{\eta}}^{\mathsf{T}}\mathbf{S} + \tilde{\tilde{\mathbf{N}}}, \tag{11}$$

where $\tilde{\tilde{\mathbf{N}}} \triangleq \alpha \mathbf{a}_{\mathtt{r}}\mathbf{a}_{\mathtt{t}}^{\mathsf{H}}\mathbf{W}\mathbf{\Gamma}\mathbf{S} + \tilde{\mathbf{N}}$. It is observed that for an arbitrary $\mathbf{W}\mathbf{\Gamma}$, the sensing beamformer $\mathbf{v} = \mathbf{a}_{\mathtt{t}}$ maximizes the received echo power at the BS. Furthermore, the MRT beamformer toward the communication users is $\mathbf{W} = \hat{\mathbf{H}} =$

$[\hat{\mathbf{h}}_1, \ldots, \hat{\mathbf{h}}_k, \ldots, \hat{\mathbf{h}}_K]$, where $\hat{\mathbf{h}}_k$ is given in (6). Thus, $\mathbf{F}$ and $\mathbf{f}_k$ can be rewritten as

$$\mathbf{F} = \hat{\mathbf{H}}\boldsymbol{\Gamma} + \mathbf{a}_{\mathtt{t}}\bar{\boldsymbol{\eta}}^{\mathsf{T}}, \ \mathbf{f}_k = \sqrt{\gamma_k}\hat{\mathbf{h}}_k + \sqrt{\eta_k}\mathbf{a}_{\mathtt{t}}. \tag{12}$$

A. Communications Sum Rate

We rewrite (5) as

$$y_{k\ell} = \mathtt{DS}_k s_{k\ell} + \mathtt{BU}_k s_{k\ell} + \sum\nolimits_{j\neq k} \mathtt{UI}_{kj} s_{\ell j} + n_{k\ell}, \tag{13}$$

where $\mathtt{DS}_k \triangleq \mathbb{E}\{\mathbf{h}_k^{\mathsf{H}}\mathbf{f}_k\}$, $\mathtt{BU}_k \triangleq \mathbf{h}_k^{\mathsf{H}}\mathbf{f}_k - \mathbb{E}\{\mathbf{h}_k^{\mathsf{H}}\mathbf{f}_k\}$, and $\mathtt{UI}_{kj} \triangleq \mathbf{h}_k^{\mathsf{H}}\mathbf{f}_j$ represent the desired signal, beamforming uncertainty, and inter-user interference, respectively. From (13), the achievable rate of the k-th user over L time slots is given by

$$R_k = \bar{\tau}\log_2\Big(1 + \frac{|\mathtt{DS}_k|^2}{\mathbb{E}\left\{|\mathtt{BU}_k|^2\right\} + \sum\limits_{j\neq k}\mathbb{E}\left\{|\mathtt{UI}_{kj}|^2\right\} + \sigma_{\mathtt{u}}^2}\Big), \tag{14}$$

where $\bar{\tau} \triangleq \left(\tau_{\mathtt{c}} - \tau_{\mathtt{p}}\right)/\tau_{\mathtt{c}}$. The following theorem gives a closed-form expression for the achievable rate of communications users.

Theorem 1: The achievable rate of the k-th user with the MRT precoder is given in the following closed-form:

$$R_k(\boldsymbol{\gamma}, \bar{\boldsymbol{\eta}}) = \bar{\tau}\log_2\left(1 + \frac{N_{\mathtt{t}}^2\xi_k^2\gamma_k}{N_{\mathtt{t}}\beta_k\sum_{j=1}^{K}(\xi_j\gamma_j + \eta_j) + \sigma_{\mathtt{u}}^2}\right), \tag{15}$$

where ξ_k and ϵ_k are given in (7) and (8), respectively, $\boldsymbol{\gamma} \triangleq [\gamma_1, \ldots, \gamma_k, \ldots, \gamma_K]^{\mathsf{T}}$, and $\bar{\boldsymbol{\eta}} \triangleq [\sqrt{\eta_1}, \ldots, \sqrt{\eta_k}, \ldots, \sqrt{\eta_K}]^{\mathsf{T}}$.

Proof: See Appendix A

Remark 1: It is observed from (15) that the sensing power factors $\{\eta_j\}$ lead to larger beamforming gain uncertainty and inter-user interference, causing performance degradation to the communications subsystem. However, note that the numerator of the SINR term in (15) increases with $N_{\mathtt{t}}^2$, while the denominator only increases with $N_{\mathtt{t}}$. Therefore, the massive MIMO JCAS system becomes free of interference as $N_{\mathtt{t}} \to \infty$, which is similar to conventional massive MIMO systems without any sensing function. In other words, deploying a very large number of antennas can mitigate the effect of sensing on communications.

B. Sensing CRB

The CRB serves as a lower bound on the variance of unbiased estimators. In the following, we characterize the CRB for estimating the target's angle θ in the sensing subsystem.

Theorem 2: The closed-form CRB for estimating the target angle θ is given as

$$\mathtt{CRB}(\boldsymbol{\gamma}, \bar{\boldsymbol{\eta}}) = \frac{\bar{\sigma}_{\mathtt{r}}^2}{\left(N_{\mathtt{t}}\left\|\dot{\mathbf{a}}_{\mathtt{r}}\right\|^2 + N_{\mathtt{r}}\left\|\dot{\mathbf{a}}_{\mathtt{t}}\right\|^2\right)\boldsymbol{\xi}^{\mathsf{T}}\boldsymbol{\gamma} + N_{\mathtt{t}}^2\left\|\dot{\mathbf{a}}_{\mathtt{r}}\right\|^2\left\|\bar{\boldsymbol{\eta}}\right\|^2}, \tag{16}$$

where $\boldsymbol{\xi} = [\xi_1, \ldots, \xi_k, \ldots, \xi_K]^{\mathsf{T}}$, $\bar{\sigma}_{\mathtt{r}}^2 \triangleq \frac{\sigma_{\mathtt{r}}^2}{2|\alpha|^2 L}$, and

$$\dot{\mathbf{a}}_{\mathtt{x}} = \left[-j\frac{N_{\mathtt{x}}-1}{2}\pi\cos(\theta), \ldots, j\frac{N_{\mathtt{x}}-1}{2}\pi\cos(\theta)\right]^{\mathsf{T}} \odot \mathbf{a}_{\mathtt{x}}, \tag{17}$$

with $\odot$ denoting the Hadamard product of two vectors.

Proof: See Appendix B. □

Remark 2: For fixed $(\boldsymbol{\gamma}, \bar{\boldsymbol{\eta}})$, it is clear that $\mathtt{CRB}(\boldsymbol{\gamma}, \bar{\boldsymbol{\eta}}) \to 0$ as $N_{\mathtt{t}} \to \infty$.

It can be concluded from Remarks 1 and 2 that both the communications and sensing performance is improved when $N_{\mathtt{t}}$ increases. Furthermore, the mutual interference between the two functions is also mitigated as $N_{\mathtt{t}}$ grows.

IV. Power Allocation

With the derived achievable rate and CRB, we are interested in a communications-centric design of the system that maximizes the sum rate while ensuring the sensing CRB and power constraints. Based on (37) and the fact that trace $\left(\mathbf{a}_{\mathtt{t}}\mathbf{a}_{\mathtt{t}}^{\mathsf{H}}\right) = N_{\mathtt{t}}$, the total transmit power is

$$\mathbb{E}\left\{\text{trace}\left(\mathbf{F}\mathbf{F}^{\mathsf{H}}\right)\right\} = N_{\mathtt{t}}\left(\boldsymbol{\xi}^{\mathsf{T}}\boldsymbol{\gamma} + \left\|\bar{\boldsymbol{\eta}}\right\|^2\right) \triangleq P_{\mathtt{opt}}. \tag{18}$$

Thus, the power allocation problem is formulated as

$$\underset{\boldsymbol{\gamma}, \bar{\boldsymbol{\eta}}}{\text{maximize}} \quad \sum_{k=1}^{K} R_k(\boldsymbol{\gamma}, \bar{\boldsymbol{\eta}}) \tag{19a}$$

$$\text{subject to} \quad \mathtt{CRB}(\boldsymbol{\gamma}, \bar{\boldsymbol{\eta}}) \leq \mathtt{CRB}_{\theta}^{0}, \tag{19b}$$

$$\boldsymbol{\xi}^{\mathsf{T}}\boldsymbol{\gamma} + \left\|\bar{\boldsymbol{\eta}}\right\|^2 \leq \frac{P_{\mathtt{t}}}{N_{\mathtt{t}}}, \tag{19c}$$

where $\mathtt{CRB}_{\theta}^{0}$ is a threshold to guarantee the sensing performance. While the constraints are convex, the objective function (19a) is non-convex. Next, we propose an efficient solution to address (19) by leveraging the SCA method [22].

A. Proposed Solution

Concave approximation of (19a)*:* To approximate $R_k(\boldsymbol{\gamma}, \bar{\boldsymbol{\eta}})$, we use the following inequality [23]:

$$\begin{aligned}\ln\left(1 + \frac{x}{y}\right) \geq& \ln\left(1 + \frac{x^{(i)}}{y^{(i)}}\right) + 2\frac{x^{(i)}}{x^{(i)} + y^{(i)}} \\ &- \frac{(x^{(i)})^2}{x^{(i)} + y^{(i)}}\frac{1}{x} - \frac{x^{(i)}}{(x^{(i)} + y^{(i)})y^{(i)}}y,\end{aligned} \tag{20}$$

where $x^{(i)}$ and $y^{(i)}$ are feasible points for x and y at the i-th iteration, respectively. We can see that the right-hand side (RHS) of (20) is a concave lower bound for $\ln\left(1 + x/y\right)$. Using (20), $R_k(\boldsymbol{\gamma}, \bar{\boldsymbol{\eta}})$ in (15) is lower bounded at iteration i by

$$\begin{aligned}R_k^{(i)}(\boldsymbol{\gamma}, \bar{\boldsymbol{\eta}}) =& \frac{\bar{\tau}}{\ln 2}\Big[A_k^{(i)} - \frac{B_k^{(i)}}{N_{\mathtt{t}}^2\xi_k^2}\frac{1}{\gamma_k} \\ &- C_k^{(i)}\Big(N_{\mathtt{t}}\beta_k\sum_{j=1}^{K}(\gamma_j\xi_j + \eta_j) + \sigma_{\mathtt{u}}^2\Big)\Big],\end{aligned} \tag{21}$$

where

$$\begin{aligned}A_k^{(i)} \triangleq& \ln\left(1 + \frac{N_{\mathtt{t}}^2\xi_k^2\gamma_k^{(i)}}{N_{\mathtt{t}}\beta_k\sum_{j=1}^{K}(\gamma_j^{(i)}\xi_j + \eta_j^{(i)}) + \sigma_{\mathtt{u}}^2}\right) \\ &+ 2\frac{N_{\mathtt{t}}^2\xi_k^2\gamma_k^{(i)}}{N_{\mathtt{t}}^2\xi_k^2\gamma_k^{(i)} + N_{\mathtt{t}}\beta_k\sum_{j=1}^{K}(\gamma_j^{(i)}\xi_j + \eta_j^{(i)}) + \sigma_{\mathtt{u}}^2}\end{aligned}$$

$$B_k^{(i)} \triangleq \frac{\left(N_{\mathtt{t}}^2\xi_k^2\gamma_k^{(i)}\right)^2}{N_{\mathtt{t}}^2\xi_k^2\gamma_k^{(i)} + N_{\mathtt{t}}\beta_k\sum_{j=1}^{K}(\gamma_j^{(i)}\xi_j + \eta_j^{(i)}) + \sigma_{\mathtt{u}}^2}$$

Algorithm 1 Iterative Algorithm for the Power Allocation Problem (19)

Initialization: Set $i := 1$ and generate an initial feasible value for $(\boldsymbol{\gamma}^{(i)}, \bar{\boldsymbol{\eta}}^{(i)}, \varphi^{(i)})$ to constraints in (26)

1: **repeat**
2: Solve (26) to obtain the optimal solution $(\boldsymbol{\gamma}^*, \bar{\boldsymbol{\eta}}^*, \varphi^*)$.
3: Update $(\boldsymbol{\gamma}^{(i)}, \bar{\boldsymbol{\eta}}^{(i)}, \varphi^{(i)}) := (\boldsymbol{\gamma}^*, \bar{\boldsymbol{\eta}}^*, \varphi^*)$
4: Set $i := i + 1$
5: **until** convergence
6: **Output:** $(\boldsymbol{\gamma}^*, \bar{\boldsymbol{\eta}}^*)$.

$$C_k^{(i)} \triangleq N_{\mathtt{t}}^2 \xi_k^2 \gamma_k^{(i)} \Big/ \Big[\big(N_{\mathtt{t}}^2 \xi_k^2 \gamma_k^{(i)} + N_{\mathtt{t}} \beta_k \sum_{j=1}^{K} (\gamma_j^{(i)} \xi_j + \eta_j^{(i)}) + \sigma_{\mathtt{u}}^2 \big) \big(N_{\mathtt{t}} \beta_k \sum_{j=1}^{K} (\gamma_j^{(i)} \xi_j + \eta_j^{(i)}) + \sigma_{\mathtt{u}}^2 \big) \Big]. \tag{22}$$

Convex approximation of (19b)*:* The closed-form CRB in (16) is convenient for performance analysis as well as solving (19). However, it is only valid for the symmetric forms of $\mathbf{a}_{\mathtt{t}}$ and $\mathbf{a}_{\mathtt{r}}$ defined in (17). Thus, to address (19b), we use the form of the CRB in (36) in Appendix B for a general array model, i.e. $\mathtt{CRB}(\boldsymbol{\gamma}, \bar{\boldsymbol{\eta}}) = \frac{\bar{\sigma}_{\mathtt{r}}^2 T_1(\boldsymbol{\gamma}, \bar{\boldsymbol{\eta}})}{T_2(\boldsymbol{\gamma}, \bar{\boldsymbol{\eta}}) T_1(\boldsymbol{\gamma}, \bar{\boldsymbol{\eta}}) - |T_3(\boldsymbol{\gamma}, \bar{\boldsymbol{\eta}})|^2}$. The product of T_1 and T_2 makes constraint (19b) impossible to be tackled directly. Alternatively, we introduce a new variable $\varphi \in \mathbb{R}_+$ to transform the constraint into the following equivalent form:

$$(19b) \Leftrightarrow \begin{cases} \dfrac{\bar{\sigma}_{\mathtt{r}}^2}{\mathtt{CRB}_\theta^0} T_1(\boldsymbol{\gamma}, \bar{\boldsymbol{\eta}}) + |T_3(\boldsymbol{\gamma}, \omega)|^2 \le \varphi^2 & \text{(23a)} \\ \varphi^2 \le T_1(\boldsymbol{\gamma}, \bar{\boldsymbol{\eta}}) T_2(\boldsymbol{\gamma}, \bar{\boldsymbol{\eta}}). & \text{(23b)} \end{cases}$$

To iteratively convexify (23a), we approximate φ^2 as:

$$\frac{\bar{\sigma}_{\mathtt{r}}^2}{\mathtt{CRB}_\theta^0} T_1(\boldsymbol{\gamma}, \bar{\boldsymbol{\eta}}) + |T_3(\boldsymbol{\gamma}, \omega)|^2 \le 2\varphi^{(i)} \varphi - (\varphi^{(i)})^2, \tag{24}$$

where $2\varphi^{(i)}\varphi - (\varphi^{(i)})^2$ is a concave lower bound of φ^2 around the point $\varphi^{(i)}$. It is clear that $T_1(\boldsymbol{\gamma}, \bar{\boldsymbol{\eta}})$ and $T_2(\boldsymbol{\gamma}, \bar{\boldsymbol{\eta}})$ are linear with respect to $(\boldsymbol{\gamma}, \bar{\boldsymbol{\eta}})$. As a result, we cast (23b) into a second-order cone (SOC) constraint as follows:

$$\big\| \varphi,\ 0.5\big(T_1(\boldsymbol{\gamma}, \bar{\boldsymbol{\eta}}) - T_2(\boldsymbol{\gamma}, \bar{\boldsymbol{\eta}})\big) \big\|_2 \le 0.5\big(T_1(\boldsymbol{\gamma}, \bar{\boldsymbol{\eta}}) + T_2(\boldsymbol{\gamma}, \bar{\boldsymbol{\eta}})\big). \tag{25}$$

In summary, we solve the following approximate convex version of (19) at iteration i:

$$\underset{\boldsymbol{\gamma}, \bar{\boldsymbol{\eta}}, \varphi}{\text{maximize}} \quad \sum_{k=1}^{K} R_k^{(i)}(\boldsymbol{\gamma}, \bar{\boldsymbol{\eta}}) \tag{26a}$$

$$\text{subject to} \quad (19c), (24), (25). \tag{26b}$$

B. Overall Algorithm and Complexity Analysis

The proposed algorithm to solve problem (19) is summarized in Algorithm 1. We iteratively solve the approximate convex program (26) to find the optimal solution, which acts as the feasible point for the next iteration. The procedure is repeated until convergence, as determined by the difference in the communication sum rate between two successive iterations. Based on [24], Algorithm 1 is guaranteed to produce a sequence of better solutions with non-decreasing values for the objective function, i.e. $\sum_{k=1}^{K} R_k^{(i)}(\boldsymbol{\gamma}, \bar{\boldsymbol{\eta}}) \le \sum_{k=1}^{K} R_k^{(i+1)}(\boldsymbol{\gamma}, \bar{\boldsymbol{\eta}})$. The sequence of the non-decreasing values is bounded by (19c), and thus Algorithm 1 will converge to at least a local optimum of (19). The convex program (26) includes $2K + 1$ scalar decision variables and 3 linear constraints. Using the interior-point method [22, Chapter 6], the worst-case of per-iteration complexity of Algorithm 1 is $\mathcal{O}\big(8\sqrt{3}K^3\big)$.

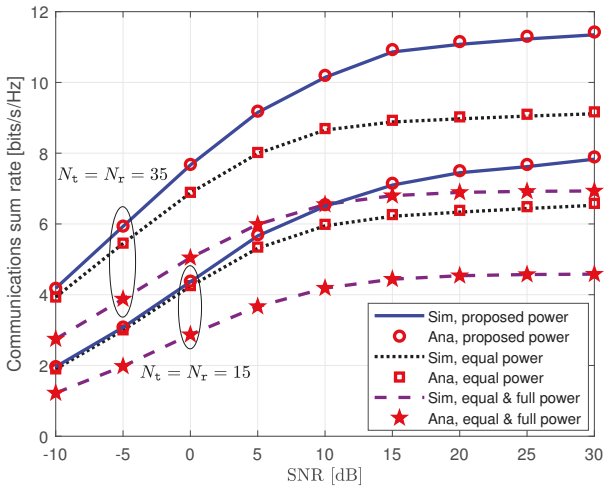

Fig. 1. Communications sum rates of the proposed power allocation scheme.

V. Simulation Results

In this section we provide numerical results to validate the theoretical findings and proposed design. We consider a scenario where the users are uniformly and randomly distributed within a cell of radius of 500 meters (m), where the BS is located at the center. We assume that no user is closer to the BS than $r_{\mathtt{h}} = 100$ m. The large-scale fading parameters are computed as $\beta_k = z_k/(r_k/r_{\mathtt{h}})^{\nu}$, where z_k is a log-normal random variable with standard deviation $\sigma_{\mathtt{shadow}} = 8$ dB, r_k is the distance between the k-th user and the BS, and $\nu = 3.2$ is the path loss exponent [10]. We set $N_{\mathtt{t}} = N_{\mathtt{r}} = \{15, 35\}$, $K = 4$, $L = 30$, and $P_{\mathtt{t}} = 30$ dBm. During the uplink training phase, we employ $\tau_{\mathtt{p}} = 10$, $\tau_{\mathtt{c}} = 100$, and $p_{\mathtt{p}} = 10$ dBm. The communications and sensing SNRs are defined as $\mathrm{SNR}_{\mathtt{com}} = P_{\mathtt{t}}/\sigma_{\mathtt{u}}^2$ and $\mathrm{SNR}_{\mathtt{sen}} = P_{\mathtt{t}}/\bar{\sigma}_{\mathtt{r}}^2$ [6], respectively. We assume that the target angle is $\theta = 0^\circ$ and set $\mathrm{SNR}_{\mathtt{sen}} = 5$ dB, $\mathtt{CRB}_\theta^0 = 10^{-3}$. For comparison, we consider two approaches referred to as "equal power" and "equal & full power." In the former, the power factors $(\tilde{\boldsymbol{\gamma}}, \tilde{\boldsymbol{\eta}})$ are set such that $\tilde{\gamma}_1 = \ldots = \tilde{\gamma}_K$, $\tilde{\eta}_1 = \ldots = \tilde{\eta}_K$, and $N_{\mathtt{t}}(\boldsymbol{\xi}^{\mathtt{T}}\tilde{\boldsymbol{\gamma}} + \sum_{k=1}^{K} \tilde{\eta}_k) = P_{\mathtt{opt}}$, where $P_{\mathtt{opt}}$ is given in (18) and obtained with the optimized power factors. In the latter, we employ power factors $(\hat{\boldsymbol{\gamma}}, \hat{\boldsymbol{\eta}})$ with $\hat{\gamma}_1 = \ldots = \hat{\gamma}_K$, $\hat{\eta}_1 = \ldots = \hat{\eta}_K$, and $N_{\mathtt{t}}(\boldsymbol{\xi}^{\mathtt{T}}\hat{\boldsymbol{\gamma}} + \sum_{k=1}^{K} \hat{\eta}_k) = P_{\mathtt{t}}$. Both benchmarks have a total transmit power larger than or equal to the proposed design.

In Fig. 1, we show the achievable sum rates obtained based on both our closed-form expressions and Monte-Carlo simulations of the proposed power allocation scheme compared with the benchmarks. It is observed that for all the considered scenarios, the analytical and simulation results match well with

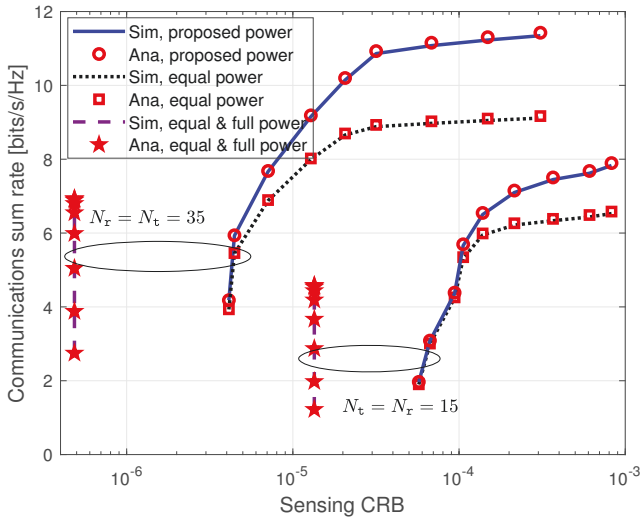

Fig. 2. Communications sum rates and sensing CRBs for $\text{SNR}_{\text{com}} = [-10, 30]$ dB.

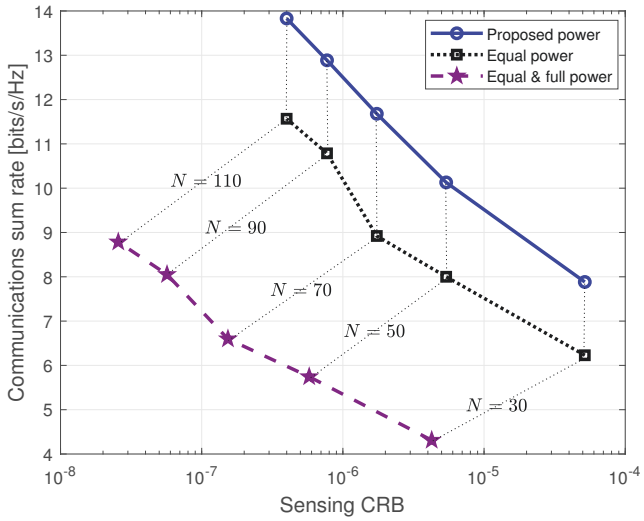

Fig. 3. Communications sum rates and sensing CRBs as N increases, with $N_t = N_r = N/2$ and $\text{SNR}_{\text{com}} = 20$ dB.

each other, validating our theoretical findings. A comparison of the considered power allocation methods demonstrates that the proposed approach offers the highest sum rate, and the gains become more significant as the number of antennas increases. In particular, despite using the entire power budget for transmission, the "equal & full power" scheme performs far worse than the others. This is because of the large interference introduced by the sensing on the communications.

In Fig. 2 and Fig. 3, we show the tradeoff between the communications sum rate and sensing CRBs of the compared approaches for various choices of (N_t, N_r) and SNR_{com}. In both figures, it is clear that the considered algorithms guarantee the design constraint $\text{CRB} \leq \text{CRB}_\theta^0 = 10^{-3}$. With a larger power fraction allocated to sensing, the "equal & full power" scheme achieves a much lower CRB than the other approaches. However, this comes at the cost of poor communication rates. In contrast, the proposed power allocation method offers the best communications–sensing performance tradeoff. For example, with $N_t = N_r = 35$ and $\text{CRB} = 10^{-4}$, the proposed design offers 24% higher sum rate compared with the "equal power" design. It is observed in Fig. 3 that as the number of antennas increases, all the considered approaches have lower CRBs and increased sum rates, verifying our theoretical findings in Remarks 1 and 2.

VI. Conclusion

We investigated mono-static multiuser massive MIMO JCAS systems with linear MRT precoding. To characterize the system performance, we derived closed-form expressions for the achievable communications sum rate and sensing CRB for estimating the target angle. The analytical findings reveal important properties about JCAS operations in massive MIMO scenarios such as the subsystems' mutual interference and the impact of the large number of antennas. We proposed an algorithm for power allocation among the precoders for the communications users and the sensed target to maximize the users' sum rate with a constraint on the CRB. Our theoretical finding and proposed algorithm were verified by numerical results, which show superior communications and sensing performance in massive MIMO JCAS systems. Our future work will consider additional radar sensing parameters such as the range and range-rate.

Acknowledgement

This work was supported in part by the Research Council of Finland through 6G Flagship under Grant 346208 and through project DIRECTION under Grant 354901, EERA Project under Grant 332362, Business Finland, Keysight, MediaTek, Siemens, Ekahau, and Verkotan via project 6GLearn, and U.S. National Science Foundation grant CCF-2225575.

Appendix A
Proof of Theorem 1

In the following, we compute $|\mathtt{DS}_k|^2$, $\mathbb{E}\left\{|\mathtt{BU}_k|^2\right\}$, and $\mathbb{E}\left\{|\mathtt{UI}_{kj}|^2\right\}$. Using (12), we first have

$$\begin{aligned}\mathbf{h}_k^{\mathsf{H}}\mathbf{f}_i &= \left(\hat{\mathbf{h}}_k + \mathbf{e}_k\right)^{\mathsf{H}}\left(\sqrt{\gamma_i}\hat{\mathbf{h}}_i + \sqrt{\eta_i}\mathbf{a}_t\right) \\ &= \sqrt{\gamma_i}\hat{\mathbf{h}}_k^{\mathsf{H}}\hat{\mathbf{h}}_i + \sqrt{\eta_i}\hat{\mathbf{h}}_k^{\mathsf{H}}\mathbf{a}_t + \mathbf{e}_k^{\mathsf{H}}(\sqrt{\gamma_i}\hat{\mathbf{h}}_i + \sqrt{\eta_i}\mathbf{a}_t) \quad (27)\end{aligned}$$

for $k, i = 1, \ldots, K$. We note that

$$\mathbb{E}\left\{\sqrt{\eta_i}\hat{\mathbf{h}}_k^{\mathsf{H}}\mathbf{a}_t + \mathbf{e}_k^{\mathsf{H}}(\sqrt{\gamma_i}\hat{\mathbf{h}}_i + \sqrt{\eta_i}\mathbf{a}_t)\right\} = 0, \forall k, i, \quad (28)$$

because $\mathbf{e}_k$ and $\hat{\mathbf{h}}_i$ are independent for $k \neq i$, and both have zero means.

- Computation of $|\mathtt{DS}_k|^2$: Using (27) and (28), we have

$$|\mathtt{DS}_k|^2 = \gamma_k \left|\mathbb{E}\left\{\|\hat{\mathbf{h}}_k\|^2\right\}\right|^2 = N_t^2\xi_k^2\gamma_k. \quad (29)$$

- Computation of $\mathbb{E}\left\{|\mathtt{BU}_k|^2\right\}$: We have

$$\begin{aligned}\mathbb{E}\left\{|\mathtt{BU}_k|^2\right\} &= \mathbb{E}\left\{|\mathbf{h}_k^{\mathsf{H}}\mathbf{f}_k|^2\right\} - |\mathbb{E}\{\mathbf{h}_k^{\mathsf{H}}\mathbf{f}_k\}|^2 \\ &= \gamma_k\mathbb{E}\left\{\|\hat{\mathbf{h}}_k\|^4\right\} + \eta_k\mathbb{E}\left\{|\hat{\mathbf{h}}_k^{\mathsf{H}}\mathbf{a}_t|^2\right\} \\ &\quad + \mathbb{E}\left\{|\mathbf{e}_k^{\mathsf{H}}(\sqrt{\gamma_k}\hat{\mathbf{h}}_k + \sqrt{\eta_k}\mathbf{a}_t)|^2\right\} - |\mathbb{E}\{\mathbf{h}_k^{\mathsf{H}}\mathbf{f}_k\}|^2. \quad (30)\end{aligned}$$

Noting that the elements of $\mathbf{a}_{\mathtt{t}}$ are deterministic with unit modulus and $\hat{\mathbf{h}}_k \sim \mathcal{CN}(0, \xi_k \mathbf{I}_{N_{\mathtt{t}}})$, we have

$$\mathbb{E}\left\{\|\hat{\mathbf{h}}_k\|^4\right\} = N_{\mathtt{t}}(N_{\mathtt{t}}+1)\xi_k^2, \tag{31}$$

$$\mathbb{E}\left\{|\hat{\mathbf{h}}_k^{\mathsf{H}}\mathbf{a}_{\mathtt{t}}|^2\right\} = \mathbb{E}\left\{\left\|\hat{\mathbf{h}}_k\right\|^2\right\} = N_{\mathtt{t}}\xi_k, \tag{32}$$

$$\mathbb{E}\left\{|\mathbf{e}_k^{\mathsf{H}}(\sqrt{\gamma_k}\hat{\mathbf{h}}_k + \sqrt{\eta_k}\mathbf{a}_{\mathtt{t}})|^2\right\} = \gamma_k \mathbb{E}\left\{\left|\mathbf{e}_k^{\mathsf{H}}\hat{\mathbf{h}}_k\right|^2\right\} + \eta_k \mathbb{E}\left\{|\mathbf{e}_k^{\mathsf{H}}\mathbf{a}_{\mathtt{t}}|^2\right\} = N_{\mathtt{t}}\epsilon_k\left(\gamma_k\xi_k + \eta_k\right). \tag{33}$$

From (29)–(33) and the fact that $\xi_k + \epsilon_k = \beta_k$, we obtain

$$\mathbb{E}\left\{|\mathtt{BU}_k|^2\right\} = N_{\mathtt{t}}\beta_k\left(\xi_k\gamma_k + \eta_k\right). \tag{34}$$

• Computation of $\mathbb{E}\left\{|\mathtt{UI}_{kj}|^2\right\}$: Using the results in (32) and (33), we have

$$\mathbb{E}\left\{|\mathtt{UI}_{kj}|^2\right\} = \gamma_j \mathbb{E}\left\{\left|\hat{\mathbf{h}}_k^{\mathsf{H}}\hat{\mathbf{h}}_j\right|^2\right\} + \eta_j \mathbb{E}\left\{\left|\hat{\mathbf{h}}_k^{\mathsf{H}}\mathbf{a}_{\mathtt{t}}\right|^2\right\} + \mathbb{E}\left\{\left|\mathbf{e}_k^{\mathsf{H}}(\sqrt{\gamma_j}\hat{\mathbf{h}}_j + \sqrt{\eta_j}\mathbf{a}_{\mathtt{t}})\right|^2\right\} = N_{\mathtt{t}}\beta_k(\gamma_j\xi_j + \eta_j). \tag{35}$$

From (29), (34), and (35), we obtain (15).

Appendix B
Proof of Theorem 2

We start from the general CRB for θ as [6]

$$\mathtt{CRB}(\boldsymbol{\gamma}, \bar{\boldsymbol{\eta}}) = \frac{\bar{\sigma}_{\mathtt{r}}^2 T_1(\boldsymbol{\gamma}, \bar{\boldsymbol{\eta}})}{T_2(\boldsymbol{\gamma}, \bar{\boldsymbol{\eta}})T_1(\boldsymbol{\gamma}, \bar{\boldsymbol{\eta}}) - |T_3(\boldsymbol{\gamma}, \bar{\boldsymbol{\eta}})|^2}, \tag{36}$$

where $\bar{\sigma}_{\mathtt{r}}^2 \triangleq \frac{\sigma_{\mathtt{r}}^2}{2|\alpha|^2 L}$, $T_1(\boldsymbol{\gamma}, \bar{\boldsymbol{\eta}}) \triangleq \text{trace}\left(\mathbf{A}^{\mathsf{H}}\mathbf{A}\mathbf{R}_x\right)$, $T_2(\boldsymbol{\gamma}, \bar{\boldsymbol{\eta}}) \triangleq \text{trace}\left(\dot{\mathbf{A}}^{\mathsf{H}}\dot{\mathbf{A}}\mathbf{R}_x\right)$, and $T_3(\boldsymbol{\gamma}, \bar{\boldsymbol{\eta}}) \triangleq \text{trace}\left(\dot{\mathbf{A}}^{\mathsf{H}}\mathbf{A}\mathbf{R}_x\right)$. Here, $\dot{\mathbf{A}} = \dot{\mathbf{a}}_{\mathtt{r}}\mathbf{a}_{\mathtt{t}}^{\mathsf{H}} + \mathbf{a}_{\mathtt{r}}\dot{\mathbf{a}}_{\mathtt{t}}^{\mathsf{H}}$, where $\dot{\mathbf{a}}_{\mathtt{x}}$ denotes the derivative of $\mathbf{a}_{\mathtt{x}}$ with respect to θ, and $\mathbf{R}_x$ is the covariance matrix of $\mathbf{X}$. Based on (1) and (12), and assuming that L is very large, we have

$$\mathbf{R}_x = \frac{1}{L}\mathbb{E}\left\{\mathbf{X}\mathbf{X}^{\mathsf{H}}\right\} = \mathbb{E}\left\{\hat{\mathbf{H}}\boldsymbol{\Gamma}^2\hat{\mathbf{H}}^{\mathsf{H}} + \|\bar{\boldsymbol{\eta}}\|^2\mathbf{a}_{\mathtt{t}}\mathbf{a}_{\mathtt{t}}^{\mathsf{H}}\right\} = \boldsymbol{\xi}^{\mathsf{T}}\boldsymbol{\gamma}\mathbf{I}_{N_{\mathtt{t}}} + \|\bar{\boldsymbol{\eta}}\|^2\mathbf{a}_{\mathtt{t}}\mathbf{a}_{\mathtt{t}}^{\mathsf{H}}. \tag{37}$$

Furthermore, with the symmetric forms of $\mathbf{a}_{\mathtt{t}}$ and $\mathbf{a}_{\mathtt{r}}$ defined in (17), we have

$$\mathbf{a}_{\mathtt{t}}^{\mathsf{H}}\dot{\mathbf{a}}_{\mathtt{t}} = \mathbf{a}_{\mathtt{r}}^{\mathsf{H}}\dot{\mathbf{a}}_{\mathtt{r}} = 0, \|\mathbf{a}_{\mathtt{t}}\|^2 = N_{\mathtt{t}}, \|\mathbf{a}_{\mathtt{r}}\|^2 = N_{\mathtt{r}}. \tag{38}$$

Using (37) and (38), we obtain

$$T_1(\boldsymbol{\gamma}, \bar{\boldsymbol{\eta}}) = N_{\mathtt{t}}N_{\mathtt{r}}\boldsymbol{\xi}^{\mathsf{T}}\boldsymbol{\gamma} + N_{\mathtt{t}}^2 N_{\mathtt{r}}\|\bar{\boldsymbol{\eta}}\|^2, \tag{39}$$

$$T_2(\boldsymbol{\gamma}, \bar{\boldsymbol{\eta}}) = \left(N_{\mathtt{t}}\|\dot{\mathbf{a}}_{\mathtt{r}}\|^2 + N_{\mathtt{r}}\|\dot{\mathbf{a}}_{\mathtt{t}}\|^2\right)\boldsymbol{\xi}^{\mathsf{T}}\boldsymbol{\gamma} + N_{\mathtt{t}}^2\|\dot{\mathbf{a}}_{\mathtt{r}}\|^2\|\bar{\boldsymbol{\eta}}\|^2, \tag{40}$$

$$T_3(\boldsymbol{\gamma}, \bar{\boldsymbol{\eta}}) = 0, \tag{41}$$

where we have omitted detailed derivations due to the limited space. We obtain (16) by substituting (39)–(41) into (36), and the proof is complete.

References

[1] F. Liu, Y. Cui, C. Masouros, J. Xu, T. X. Han, Y. C. Eldar, and S. Buzzi, "Integrated sensing and communications: Towards dual-functional wireless networks for 6G and beyond," *IEEE J. Sel. Areas Commun.*, 2022.

[2] F. Liu, C. Masouros, A. Li, H. Sun, and L. Hanzo, "MU-MIMO communications with MIMO radar: From co-existence to joint transmission," *IEEE Trans. Wireless Commun.*, vol. 17, no. 4, pp. 2755–2770, 2018.

[3] X. Liu, T. Huang, N. Shlezinger, Y. Liu, J. Zhou, and Y. C. Eldar, "Joint transmit beamforming for multiuser MIMO communications and MIMO radar," *IEEE Trans. Signal Process.*, vol. 68, pp. 3929–3944, 2020.

[4] J. Johnston, L. Venturino, E. Grossi, M. Lops, and X. Wang, "MIMO OFDM dual-function radar-communication under error rate and beampattern constraints," *IEEE J. Sel. Areas Commun.*, vol. 40, no. 6, pp. 1951–1964, 2022.

[5] F. Liu, Y.-F. Liu, C. Masouros, A. Li, and Y. C. Eldar, "A joint radar-communication precoding design based on Cramér-Rao bound optimization," in *IEEE Radar Conf.*, 2022.

[6] F. Liu, Y.-F. Liu, A. Li, C. Masouros, and Y. C. Eldar, "Cramér-Rao bound optimization for joint radar-communication beamforming," *IEEE Trans. Signal Process.*, vol. 70, pp. 240–253, 2021.

[7] X. Song, J. Xu, F. Liu, T. X. Han, and Y. C. Eldar, "Intelligent reflecting surface enabled sensing: Cramér-Rao bound optimization," *IEEE Trans. Signal Process.*, vol. 71, pp. 2011–2026, 2023.

[8] T. L. Marzetta, "Noncooperative cellular wireless with unlimited numbers of base station antennas," vol. 9, no. 11, pp. 3590–3600, 2010.

[9] E. G. Larsson, O. Edfors, F. Tufvesson, and T. L. Marzetta, "Massive MIMO for next generation wireless systems," *IEEE Commun. Mag.*, vol. 52, no. 2, pp. 186–195, 2014.

[10] H. Q. Ngo, E. G. Larsson, and T. L. Marzetta, "Energy and spectral efficiency of very large multiuser MIMO systems," *IEEE Trans. Commun.*, vol. 61, no. 4, pp. 1436–1449, 2013.

[11] S. Buzzi, C. D'Andrea, and M. Lops, "Using massive MIMO arrays for joint communication and sensing," in *Proc. Annual Asilomar Conf. Signals, Syst., Comp.*, 2019, pp. 5–9.

[12] M. Temiz, E. Alsusa, and M. W. Baidas, "A dual-function massive MIMO uplink OFDM communication and radar architecture," *IEEE Transactions on Cognitive Communications and Networking*, vol. 8, no. 2, pp. 750–762, 2021.

[13] C. Qi, W. Ci, J. Zhang, and X. You, "Hybrid beamforming for millimeter wave MIMO integrated sensing and communications," *IEEE Commun. Lett.*, vol. 26, no. 5, pp. 1136–1140, 2022.

[14] X. Wang, Z. Fei, J. A. Zhang, and J. Xu, "Partially-connected hybrid beamforming design for integrated sensing and communication systems," vol. 70, no. 10, pp. 6648–6660, 2022.

[15] S. D. Liyanaarachchi, C. B. Barneto, T. Riihonen, M. Heino, and M. Valkama, "Joint multi-user communication and MIMO radar through full-duplex hybrid beamforming," in *IEEE Int. Online Symposium Joint Commun. & Sensing (JC&S)*, 2021.

[16] C. B. Barneto, T. Riihonen, S. D. Liyanaarachchi, M. Heino, N. González-Prelcic, and M. Valkama, "Beamformer design and optimization for full-duplex joint communication and sensing at mm-waves," *arXiv preprint arXiv:2109.05932*, 2021.

[17] N. T. Nguyen, N. Shlezinger, K.-H. Ngo, V.-D. Nguyen, and M. Juntti, "Joint communications and sensing design for multi-carrier MIMO systems," *Proc. IEEE Workshop on Statistical Signal Processing*, 2023.

[18] N. T. Nguyen, L. V. Nguyen, N. Shlezinger, Y. C. Eldar, A. L. Swindlehurst, and M. Juntti, "Joint communications and sensing hybrid beamforming design via deep unfolding," *arXiv preprint arXiv:2307.04376*, 2023.

[19] N. T. Nguyen, N. Shlezinger, Y. C. Eldar, and M. Juntti, "Multiuser MIMO wideband joint communications and sensing system with subcarrier allocation," *IEEE Trans. Signal Process.*, vol. 71, pp. 2997–3013, 2023.

[20] H. Q. Ngo, E. G. Larsson, and T. L. Marzetta, "Massive MU-MIMO downlink TDD systems with linear precoding and downlink pilots," in *Proc. Annual Allerton Conf. Commun., Contr., Computing*, 2013, pp. 293–298.

[21] C. Mollen, J. Choi, E. G. Larsson, and R. W. Heath, "Uplink performance of wideband massive MIMO with one-bit ADCs," *IEEE Trans. Wireless Commun.*, vol. 16, no. 1, pp. 87–100, 2016.

[22] A. Ben-Tal and A. Nemirovski, *Lectures on Modern Convex Optimization*. Philadelphia: MPS-SIAM Series on Optimi., SIAM, 2001.

[23] A. A. Nasir, H. D. Tuan, H. H. Nguyen, M. Debbah, and H. V. Poor, "Resource allocation and beamforming design in the short blocklength regime for URLLC," *IEEE Trans. Wireless Commun.*, vol. 20, no. 2, pp. 1321–1335, 2021.

[24] A. Beck, A. Ben-Tal, and L. Tetruashvili, "A sequential parametric convex approximation method with applications to nonconvex truss topology design problems," *J. Global Optim.*, vol. 47, no. 1, pp. 29–51, May 2010.